2.45 GHz ECR coaxial plasma source: characterization in single and multi-sources configuration

J. Lo[1], L. Latrasse[2], Ch. Laurent[1], L. Thérèse[1], B. Caillier[1], Ph. Guillot[1]

[1]*Toulouse University, CUFR J. F. Champollion, DPHE, Place de Verdun, 81012, Albi, France*
[2]*SAIREM SA., 12 Porte du Grand Lyon, Neyron 01702, France*

Investigation on the performance of a 2.45 GHz coaxial plasma source was conducted in this study through Langmuir probe diagnostic, optical emission spectroscopy and CCD imaging. The source major difference with other works resides in the use of two oppositely polarized permanent magnet mounted at the extremity of the coaxial structure. Stable plasma regimes with low sustaining power (as low as 1 W) were obtained in the pressure range of 10^{-3}~10^{-1} mbar. High density and almost uniform plasmas (constant over 150 mm) were also achieved in the case where several sources associated together in a matrix configuration.

1. Introduction

Wide range of applications put forward the importance of having large scale uniform plasmas – surface coatings, diamond deposition, polymer surface modifications, carbon nano-tubes growth etc [1, 2, 3, 4]. Multi-dipolar plasma sources which are distributed in a two or three dimensional network were proposed as far back as in 2002 [5] in order to achieve high density and uniform plasmas. Each source used was coaxial antenna head which encapsulate a permanent magnet and exploits the electron cyclotron resonance heating at microwave frequency range.

Another variant of an ECR coaxial source called *Aura source* is studied here where two magnets were used instead of one in order to obtain larger ECR surface, thus achieving uniform plasmas more easily. The performance of this source will be studied in single and multi source configuration.

2. Experimental setup

2.1. Plasma source description

A schematic diagram of the plasma source investigated is shown in Figure 1.

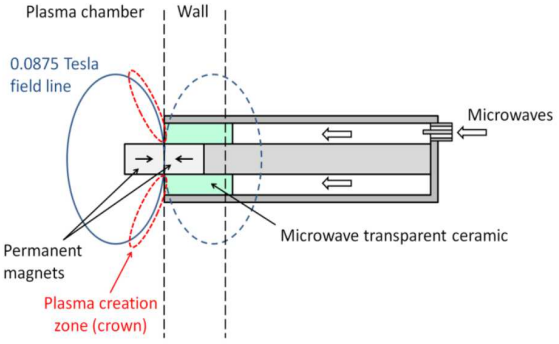

Figure 1: Schematic of ECR coaxial source with oppositely mounted magnets.

The source is described by a coaxial transmission structure with an alumina insulator separating the inner and external conductor. Axially polarized cylindrical ring magnets are encapsulated and adhered within the inner core, with one of them extending out of the coaxial structure. Each magnet was made of Samarium Cobalt *1.06±4* Tesla. Having them oppositely magnetized, the magnetic field is radial at the adhesion junction. The resulting ECR surface defined at *87.5* mTesla for *2.45* GHz microwave plasma generation is therefore much wider than coaxial plasma sources with a single magnet [6]. The electronic trapping performance of the ECR coaxial source is sought to be enhanced.

Precise power input leads to an enhanced control of the plasma, hence a better reproducibility of the plasma characteristics. This latter may appear to be critical in plasma processing where the yield performance is highly influenced by the plasma parameters. In this study, our plasma source was driven at 2.45 GHz by a solid state generator with a 200 W maximal output (SAIREM® GMS200W SM56M FST1IR). Compared to classically used generator based on magnetron technology, the solid state generator allowed precise power increment control – as low as 1 W power step – and frequency adjustment up to Δf = +/-25 MHz from the central frequency.

The applicator was designed with an optimized impedance transition from 50 Ω technologies to the plasma impedance for a wide range of conditions. The impedance matching ensured limited reflecting microwave power during operation. If needed, further impedance tuning may be ensured by adjusting the input frequency provided by the generator. Therefore, the use of supplementary impedance matching system was not necessary. Throughout this work, unless mentioned otherwise, the microwave frequency was maintained at 2.445 GHz and the power referred to the net power injected.

2.2 Single source characterization setup

For characterization purpose, the plasma source was placed on the upper side of the vacuum chamber schematized in Figure 2. Prior to any measurement, the vacuum chamber was pumped down to a base pressure of 10^{-5} mbar with a turbomolecular pump. A permanent working gas flow was then injected ensuring an interval of working pressure varying from 10^{-3} mbar to 10^{-1} mbar.

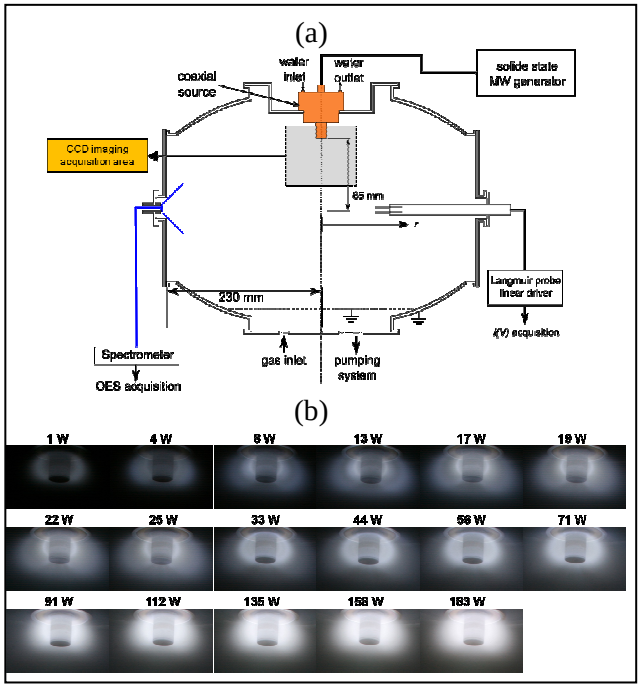

Figure 2: Experimental setup for single source (a) and plasma generated by the coaxial source at 1 Pa (b).

The plasma electrostatic characterization (plasma electronic density and temperature radial profiles) was conducted with a referenced Langmuir probe (Impedans Ltd.) positioned through a porthole. Placed at 85 mm in height from the ECR source extremity, the probe was linearly driven with a step-motor. Measurements were conducted from the source axis to the chamber wall, resulting in radial resolution of the plasma parameters. The Langmuir probe is made of two cylindrical tungsten tips: one for current–voltage (*I-V*) acquisition and another as a reference electrode for noise reduction and probe circuit impedance compensation. Data acquisition and analysis were carried out with Impedans ALP SYSTEM™. The magnetic field calculated analytically from [7] does not exceed 1 mTesla at 85 mm from the source head. At the worst case sceanario where the electronic temperature is as low as 0.5 eV, the Larmor radius is evaluated at $r_L = 2.9$ mm. The probe radius is therefore negligeable compared to the Larmor radius ($r_P << r_L$) and the classical probe theory may be used [8].

In order to identify the different species generated during the plasma ignition, the optical emission of the generated plasma in the vacuum chamber was canalized through an optical feed-through and a 600 µm optical fiber (QP600-2-SR Oceano Optics). The optical emission spectroscopy (OES) measurement with a resolution of $\Delta\lambda = 0.5$ nm was performed in the wavelength range of 200 nm to 1100 nm with a 10 µm slit-width spectrometer (Oceano Optics HR2000+). In parallel, the spatial distribution of the plasma emission was performed with a Princeton Instrument iCCD camera with a spectral sensibility ranging from 200 to 1000 nm.

3. Results and discussions

3.1. Ignition and sustaining

Breakdown in Argon and in air occurred at relatively low power input within the pressure range studied. For both gases, represented in Figure 4, the power needed in order to achieve breakdown ran as low as ~ 15 W in the 10^{-2} mbar range. Once ignited, stable plasma regimes were achieved within the power and pressure scopes of our studies. Minimal power needed to sustain the plasma is around 1 W in air and Argon.

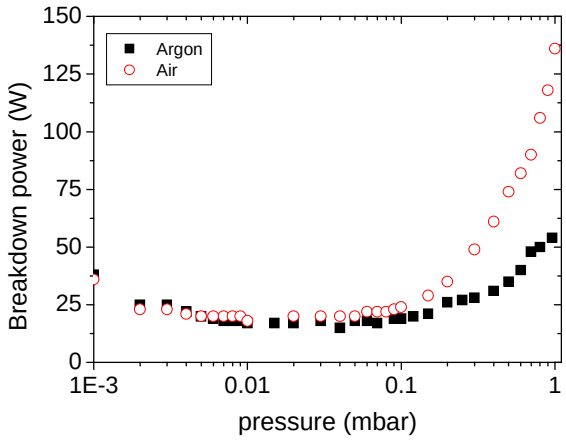

Figure 3: Breakdown power versus gas pressure

3.2. Power increase

The power increase led to the increase in optical emission intensity as well as the expansion of the optical emission zone (cf. Figure 2b). In Argon, typical optical emission spectrum is shown in Figure 4. The lines observed are dominated by $2p \rightarrow 1s$ transitions (Paschen notation) in the visible/near-IR range. The variation of the 750.4 nm line ($2p_1 \rightarrow 1s_2$) as a function of input power is shown in Figure 5. Note two distinctive increase slopes – both are exponential. A steeper slope characterize however the profile at lower power up to ~ 50 W.

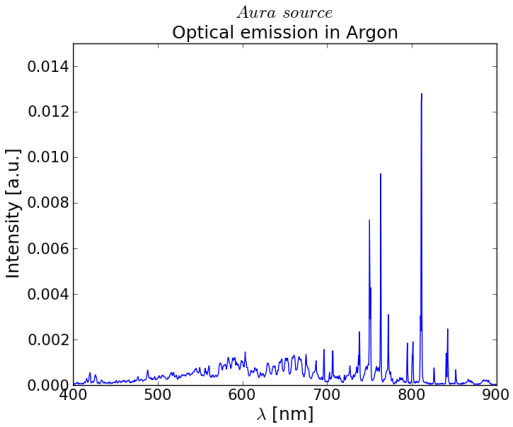

Figure 4: Emission spectrum. Argon at *1* Pa and *150* W.

The population of Argon $2p_1$ level is mainly due to electron impact excitation from the ground state [9]. Therefore, the emission intensity may be written as:

$$I_{750.4nm} = n_e n_g Q_{opt}$$

$$\text{where } Q_{opt}^{750.4nm} = \int_0^\infty \sigma_{opt}^{750.4nm} \sqrt{\frac{2E}{m_e}} f_E(E) dE$$

with n_e the electronic density, n_g the neutral gas ground state density, m_e the electron mass σ the optical emission cross section and $f_E(E)$ the electron energy distribution function. For a given transition and under Maxwellian distribution assumption, the optical emission rate coefficient $Q^{750.4nm}_{opt}$ depends solely on the electronic temperature. Measured electronic temperatures are constant as shown in Figure 6. Therefore, the two distinctive increase slopes for the 750.4 nm emission actually follow the electronic density variation shown in the same figure. Discrepancies observed are mostly due to the fact that the electronic density measurements are shown for a unique position (*r = 0* mm) whilst optical emissions from the whole chamber were measured.

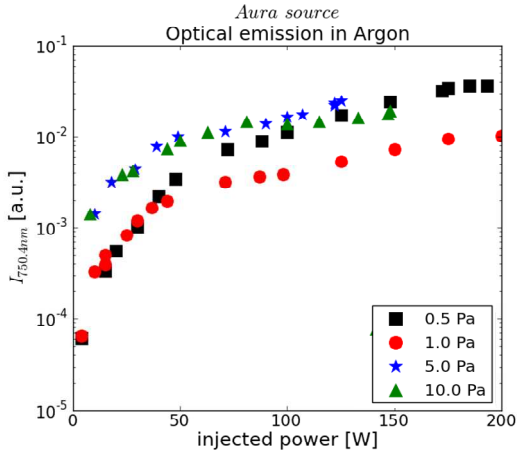

Figure 5: Optical emission at 750.4 nm as a function of injected power.

Therefore, substantial increase in electronic density with the power input was observed only up to a certain power threshold (~*50* W). Over this value, the density increase slope became lower.

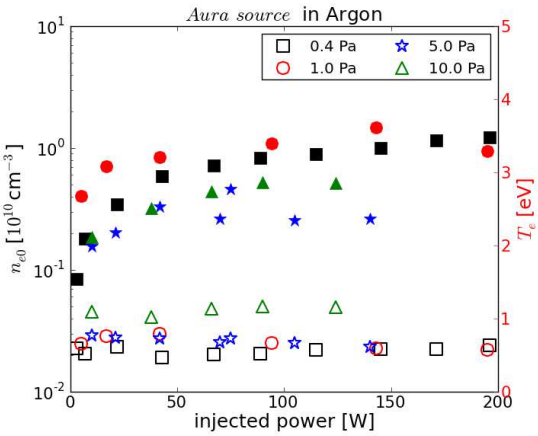

Figure 6: Electronic density (full symbols) and temperature (empty symbols) in Argon nm as a function of injected power.

3.3. Pressure increase

The pressure affects mostly the Argon metastable state presence. The line ratio between the emissions at *811.5* nm and *750.4* nm known to be good indicator of the $1s_5$ metastable state density proportion as long as photon re-absorption is negligible [10]. We assume that it is the case here.

In general the metastable state proportion increase with the pressure (cf. Figure 7), however, appearance of singular phenomena might lead to an exception of the rule. This is the case observed at *1* Pa. We attribute this to plausible the shift between discharge modes.

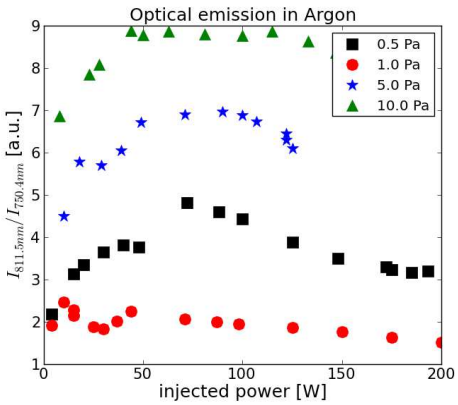

Figure 7: Ratio between transition lines at 811.5 nm and 750.4 nm as a function of power input

The intensified CCD camera images shown in Figure 8 showed the two discharge modes observed. One of them (at 5 Pa, image at right)

shows the optical emission concentrates azimuthally around the outer magnet. This zone, coincides with the area where the ionization rate is the highest shown in the work of *Hagelaar et al*. for dipolar ECR source [11]. The other image (at left) shows two zones where optical emissions are the most intense. These zones, also attributed to the ionization zone, are situated around the cylindrical magnet and at the front of the coaxial source head.

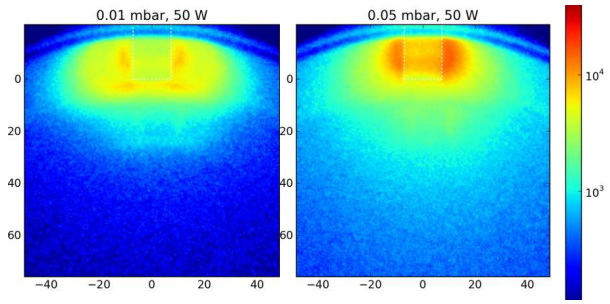

Figure 8: CCD camera images at 1 Pa (left) and 5Pa (right) for identical input power of 50 W.

4 Multisource characterization setup

Coaxial plasma sources are interesting sources as they may be organized in a matrix configuration in order to obtain uniform plasma. The characterization in multisource configuration was performed in a second vacuum chamber. The second chamber is cylindrical with a diameter of 500 mm and height of 400 mm. Up to 16 sources arranged in a square lattice – with the step size *a* – may be put on the upper side of the chamber represented in Figure 3. Each of them is independently generated by a solid state MW generator.

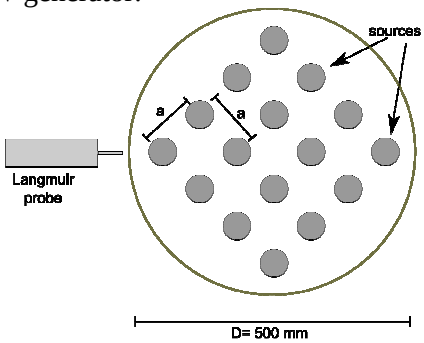

Figure 9: Top view of characterization setup in multisource configuration. The Langmuir probe was placed at 160 mm from the top.

Intensity of argon emission lines and electronic density have been studied as a function of the number sources and of the position of these sources. The plasma uniformity has been characterized and will be discussed.

5 Conclusion

An extensive study was conducted on an ECR coaxial plasma source by Langmuir probe diagnostic, optical emission spectroscopy and CCD imaging in this work. Single source results obtained in Argon were presented. Multi-sources results in argon will be presented as a function of the number of sources and position during the conference.

6 References

[1] M. Meyyappan, *J. Phys. D: Appl. Phys.* **42** (2009), 1213001
[2] A. Anders, *Surface and Coating Tech.* **200** (2005).
[3] V.G. Ralchenko, A.A. Smolin, V.I. Konov, K.F. Segeichev et al., *Diamond and Related Materials* **6** (1997).
[4] J. Hopwood, *Plasma Sources Sci. Tech.* **1** (1992)
[5] A. Lacoste, T. Lagarde, S. Béchu, Y. Arnal and J. Pelletier, *Plasma Sources Science and Technology* **11** (2002) 407-412
[6] S. Béchu, A. Soum-Glaude, A. Bès, A. Lacoste, P. Svarnas, S. Aleiferis, A. A. Ivanov, and M. Bacal, *Physics of plasmas* **20** (2013) 1101601
[7] Q.L. Peng, S.M. McMurry, J.M.D. Coey, *Journal of Magnetisme and Magnetic Materials* **268** (2004) 165-169
[8] V.A. Godyak, V.I. Demidov, *J. Phys. D: Appl. Phys.* **44** (2011) 12330
[9] J. B. Boffard, C. C. Lin, C. A. DeJoseph Jr., *J. Phys. D: Appl. Phys.* **37** (2004) R143-R161, 2004
[10] M.Schulze, A. Yanguas-Gil, A. von Keudell, P. Awakowicz, *J. Phys. D.: Appl. Phys.* **41** (2008) 1065206
[11] G. J. M. Hagelaar, K.Makasheva, L.Garrigues and J.P. Boeuf, *J. Phys. D: Appl. Phys.* **42** (2009) 194019
[12] L. Latrasse, A. Lacoste, J. Sirou, J. Pelletier, *Plasma Sources Science and Technology*, vol. **16** (2007) 7-12 and